Experimental study on the wind-turbine wake meandering inside a scale model wind farm placed in an atmospheric-boundary-layer wind tunnel

IOP Conf. Series: Journal of Physics: Conf. Series **854** (2017) 012008 doi:10.1088/1742-6596/854/1/012008

Experimental study on the wind-turbine wake meandering inside a scale model wind farm placed in an atmospheric-boundary-layer wind tunnel

N. Coudou[1,2,3], S. Buckingham[1], J. van Beeck[1]

[1]Environmental and Applied Fluid Dynamics Department, von Karman Institute for Fluid Dynamics, Waterloosesteenweg 72, 1640 Sint-Genesius-Rode, Belgium
[2]Fluids-Machines Department, Université de Mons, Rue du Joncquois 53, 7000 Mons, Belgium
[3]Institute of Mechanics, Materials and Civil Engineering, Université catholique de Louvain, Place du Levant 2, 1348 Louvain-la-Neuve, Belgium

E-mail: nicolas.coudou@vki.ac.be

Abstract. Increasing use of wind energy over the years results in more and larger clustered wind farms. It is therefore fundamental to have an in-depth knowledge of wind-turbine wakes, and especially a better understanding of the well-known but less understood wake-meandering phenomenon which causes the wake to move as a whole in both horizontal and vertical directions as it is convected downstream. This oscillatory motion of the wake is crucial for loading on downstream turbines because it increases fatigue loads and in particular yaw loads. In order to address this phenomenon, experimental investigations were carried out in an atmospheric-boundary-layer wind tunnel using a 3×3 scaled wind farm composed of three-bladed rotating wind-turbine models subject to a neutral atmospheric boundary layer (ABL) corresponding to a *slightly rough* terrain, i.e. to offshore conditions. Particle Image Velocimetry (PIV) measurements were performed in a horizontal plane, at hub height, in the wake of the three wind turbines in the wind-farm centreline. From the PIV velocity fields obtained, the wake-centrelines were determined and a spectral analysis was performed to obtain the characteristics of the wake-meandering phenomenon. In addition, Hot-Wire Anemometry (HWA) measurements were performed in the wakes of the same wind turbines to validate the PIV results. The spectral analysis performed with the spatial and temporal signals obtained from PIV and HWA measurements respectively, led to Strouhal numbers $St = fD/U_{hub} \simeq 0.20 - 0.22$.

1. Introduction

Between the years 2000 and 2015, the cumulative wind-power installations in the European Union increased from 12.9 GW to 141.6 GW [1]. Based on the European Wind Energy Association's central scenario [2], wind-energy installations could amount to over 320 GW in 2030. This important rise in the use of wind energy over the years results in more and larger clustered wind farms. It is therefore fundamental to have an in-depth knowledge of wind-turbine wakes, and especially a better understanding of the well-known but less understood wake-meandering phenomenon. Because this phenomenon causes the wake to be swept in and out of the rotor disk of downstream turbines, it is crucial for loading on these turbines since it might considerably increase fatigue loads and in particular yaw loads.

In their study performed with a two-bladed rotating wind-turbine scale model submitted to a uniform free-stream, Medici and Alfredsson [3] argued that the low-frequency vortex shedding might be responsible for the wake-meandering motion. Their measurements were supported by

a theoretical study performed by Okulov and Sørensen [4]. However, as mentioned by Larsen *et al.* [5], notable differences exist between the experimental conditions of Medici and Alfredsson's study [3], and the conditions present for a full-scale wind turbine located in the atmospheric boundary layer (ABL).

Larsen *et al.* [5] described the wake meandering process as a series of consecutive wake "releases", each advected downstream with the mean wind field and displaced, in the plane perpendicular to the mean wind direction, by the large-scale turbulent structures. In relation to the large-scale turbulent structures, the individual wake "releases" are thus presumed to behave like passive tracers [5]. España *et al.* provided experimental evidence of the role of the large eddies on the wake-meandering phenomenon behind a wind turbine modelled with a static porous disk [6–8]. The results showed that the meandering process is only generated when the turbulent length scales contained in the ABL are larger than the disk diameter, and that the meandering phenomenon cannot be attributed to the periodic vortex shedding. Further studies performed with a static porous disk located in a neutral ABL [9, 10] showed that the instantaneous horizontal wake position correlates well with the upstream transverse velocity for wavelengths larger than three times the disk diameter, whereas it is not at all the case for wavelengths smaller than twice the disk diameter. Furthermore, using two porous disks located $5D$ apart from each other highlighted an amplification of the wake meandering for the downstream turbine because of the upstream wake.

The wake of a three-bladed rotating wind-turbine scale model in onshore (*moderately rough* terrain) and offshore (*slightly rough* terrain) neutral ABL conditions was investigated by Barlas *et al.* [11]. For offshore conditions, i.e. low turbulence level ($I = 7.5\%$ at hub height), a wake meandering mechanism was detected. It was found that the Strouhal number related to this meandering was independent of the inflow velocity and was always $\mathcal{O}(0.25)$. Additional investigations were performed in offshore and onshore conditions downstream of a 3×3 wind farm but as for the single wind turbine in onshore conditions ($I = 17.5\%$ at hub height), the incoming turbulence level was too high for the meandering to survive [12].

Additional studies performed on rotating wind-turbine scale models [13–15] as well as on a hydrokinetic turbine [16] provided evidence of wake oscillations corresponding to a Strouhal number St ranging from 0.1 to 0.3. In some of these studies [14, 16], it is reported that wake meandering is caused by instabilities of the hub or tip vortices.

While most of the experimental studies about wind-turbine wake meandering concern an isolated wind-turbine scale model or two models aligned with the mean flow in a few cases, this study focusses on the three wind turbines constituting the mid row (in stream-wise direction) of a 3 x 3 scaled wind farm. In particular, the aim of the current study is to investigate if the wake meandering persists in a wind farm and to determine the characteristics of this phenomenon. In order to address that, state-of-the-art experimental techniques combined with spectral analysis are used.

2. Experimental setup

2.1. Wind turbine scale model

The three-bladed wind-turbine scale models used for the experiments have a rotor diameter of 0.15 m and a hub height of 0.13 m (Fig. 1); they can therefore be considered as representative of a scaled 2 MW offshore wind turbine (e.g. scale 1/440 of Vestas V66-2MW). The rotors, made of a HAM-STD HS1-606 airfoil, are designed by Blade Element Momentum (BEM) theory [17] with an incoming velocity of 8 m s^{-1} at hub height. Each rotor is attached to a direct current (DC) motor used as a generator which can be "counter-loaded" to extract power from the incoming wind and to control the turbine tip-speed ratio

$$TSR = \frac{\Omega \cdot R}{U_{hub}}, \tag{1}$$

where Ω is the angular velocity and U_{hub} is the mean velocity at hub height. Based on the incoming velocity at hub height ($U_{hub} = 8.3$ m s^{-1}), the tip-speed ratio of the first turbine was equal to 7.2.

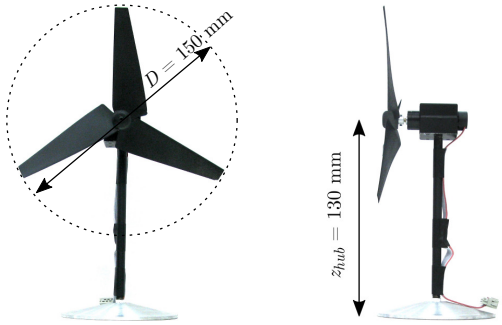

Figure 1. Wind-turbine scale model dimensions.

Figure 2. Wind farm position in configuration 1 inside the VKI Wind Engineering facility L-1B.

2.2. Wind farm setup

The 3×3 wind farm was located at the end of the test section of the VKI Wind Engineering facility L-1B (Fig. 2). The wind-turbine scale models forming the wind farm were spaced by $3D$ and $5D$ in the span-wise and stream-wise direction, respectively. Due to the limitations in the positioning of the CCD camera underneath the wind tunnel, the Particle Image Velocimetry (PIV) system was kept at its best position and the wind farm was shifted longitudinally in order to perform measurements successively in the wake of the first, the second, and the third wind turbines as depicted in Fig. 3. These changes in wind-farm positioning have no influence on the reliability of the results since the entire testing area is submitted to a fully developed ABL. Furthermore, since the PIV system remains in the same position, the comparison of the wind-turbine wakes is not affected by changes in the PIV setup.

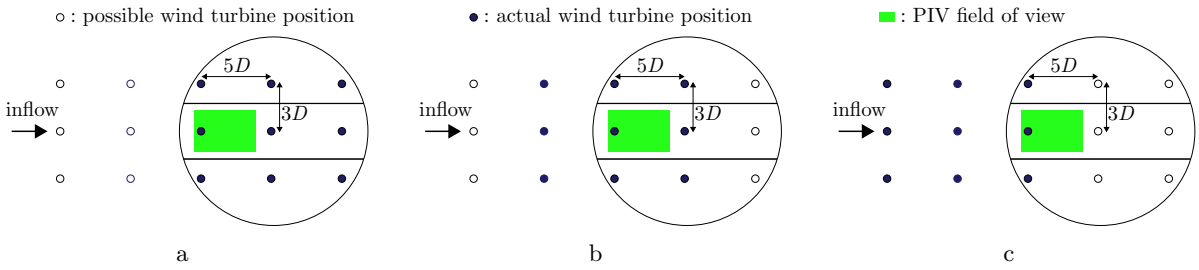

Figure 3. Wind farm position in the VKI Wind Engineering facility L-1B : sketch of configurations 1 (a), 2 (b), and 3 (c).

2.3. Incoming ABL flow

A neutral ABL was modelled in the VKI Wind Engineering facility L-1B which is a low-speed, closed-loop wind tunnel with a 2-m high, 3-m wide, and 20-m long test section. The length of the flow development section was equal to 11 m for the shortest scenario corresponding to the wind farm in configuration 3, this fetch being long enough to obtain a fully developed ABL. More information concerning the modelling of atmospheric flows in the wind tunnel L-1B can be found in [18, 19].

The ABL modelled was characterised using a one-component hot-wire anemometer and is representative of a *slightly rough* terrain, with a friction velocity $u_* = 0.33$ m s^{-1}, a full-scale aerodynamic roughness length $z_0 = 3.7 \times 10^{-3}$ m (full scale = 440 $\times$ wind-tunnel scale) and a

power law coefficient $\alpha = 0.11$ using the hub height as reference height. The main properties of the ABL modelled are compared to the VDI [20], Eurocode [21] and ESDU [22] standards for a *slightly rough* terrain (category of *type 0*) in Fig. 4a,c. The integral length scale at hub height, computed by applying the autocorrelation method on the time series and the Taylor's frozen turbulence hypothesis, is about three rotor diameters. This characteristic size of the energy-containing eddies therefore fulfils the condition presented by España *et al.* [6, 8] to observe the wake-meandering phenomenon, i.e. to have modelled turbulent scales larger than the wind-turbine rotor diameter in the inflow ABL. With regard to the spectral characteristics of the ABL, the normalised turbulent spectrum obtained at hub height (Fig. 4d) matches well with the Kansas spectrum for stream-wise component [23]. Like in [19], there is a slight overshoot in the amplitude of the peak. This overshoot is most probably caused by a low-frequency instability ($f \simeq 1.5Hz$) produced by the two contra-rotating fans of the wind tunnel. Note that this frequency is about ten times smaller than the meandering frequency.

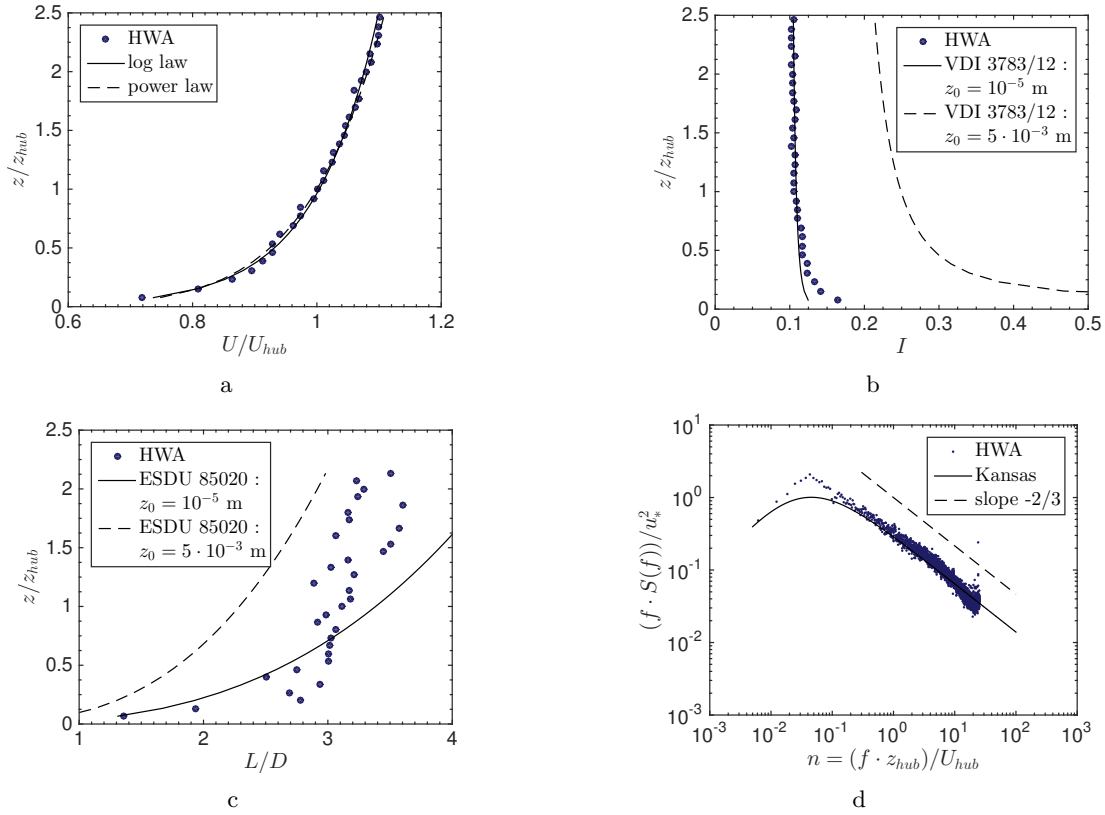

Figure 4. Vertical profiles and normalised spectrum of the atmospheric boundary layer modelled in the wind tunnel L-1B. Normalised mean velocity (a), turbulence intensity (b), integral length scales (c), normalised spectrum at hub height and Kansas spectrum [23] (d). Note that these quantities are based on the stream-wise velocity obtained by 1C-HWA measurements.

2.4. Measurement techniques

2.4.1. Particle Image velocimetry (PIV) The 2D2C-PIV technique was used to perform measurements in a horizontal plane at hub height in the wake of the wind-turbine scale models. The PIV system was set up to obtain a field of view larger than $4D$ in the stream-wise direction (Fig. 5). The seeding particles were oil droplets with a diameter of 1-5 μm. Measurements were performed using LaVision DAVIS 8 software. For each measurement, 800 pair images were acquired at a frequency of 2.5 Hz. The processing of the images was carried out using the in-house software WIDIM (WIndow Displacement and Distortion Iterative Multigrid) [24]. The

parameters used are 64×64 pixels interrogation areas and an overlap of 75%. For all fields of views, the signal-to-noise ratio was of the order of 6, what enables to have full confidence in the quality of the measurements and processing. On the basis of the uncertainty analysis procedure proposed by the International Towing Tank Conference [25] and considering a confidence interval of 95%, the uncertainty on the mean velocity was determined to equal 1.5% for hub-height velocities of 4.9 m s^{-1} and 8.3 m s^{-1}.

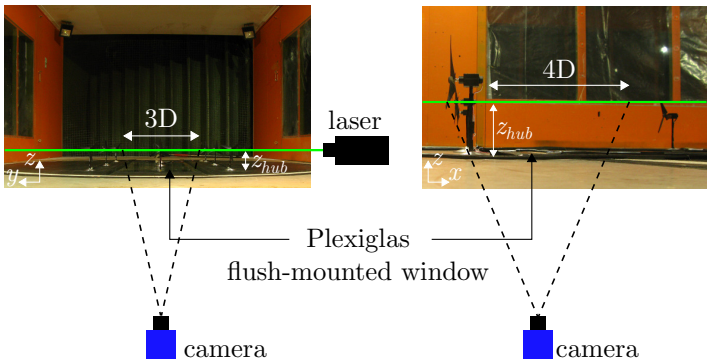

Figure 5. PIV setup in the VKI Wind Engineering facility L-1B.

2.4.2. Hot-Wire Anemometry (HWA) The hot-wire anemometer was calibrated using a low-turbulent and uniform jet created by a nozzle and controlled by a pressure difference. The calibration was carried out before and after each experimental campaign to verify the validity of the calibration throughout the experiments. The calibration curve was then fitted with a third-order polynomial in order to convert the instantaneous voltage signature into instantaneous wind velocity. The measurements were performed at $x = 2D$ downstream of each rotor disk at hub and upper tip heights. For each location, the HWA signal was acquired during 120 s with a sampling frequency of 3 kHz and low-pass filtered at 1 kHz. Based on classical uncertainty analysis [26] and considering a confidence interval of 95%, the uncertainty on the velocity was determined to be equal to 4.1% for a hub-height velocity of 7.8 m s^{-1}.

3. Estimation of the wake centreline

From the PIV measurements of the scaled wind-turbine wakes, the instantaneous deviations of the wake-centreline from its time-average location was determined using a specific processing technique based on the determination of a Gaussian function

$$f(y) = \frac{A}{2\pi\sigma} e^{-\frac{(y_i-\mu_y)^2}{2\sigma^2}} \tag{2}$$

which optimally fits the instantaneous wake velocity deficits downstream of the wind turbine [27–30]. The independent Cartesian spatial variable of the function is referred to as y_i and the shape of the function is parameterised in terms of three parameters, namely: a position parameter of the profile μ_y, a width parameter of the profile σ, and a scaling parameter A [30]. For each snapshot, the Gaussian function was fitted, through a least-squares approach, to the instantaneous wake velocity deficit profiles (Fig. 6) for stream-wise locations x_i going from $x = 0.5D$ to $x = 4D$. The wake-centre position at each location x_i was then determined from the location of the maximum of the Gaussian function fitting each wake velocity deficit profile.

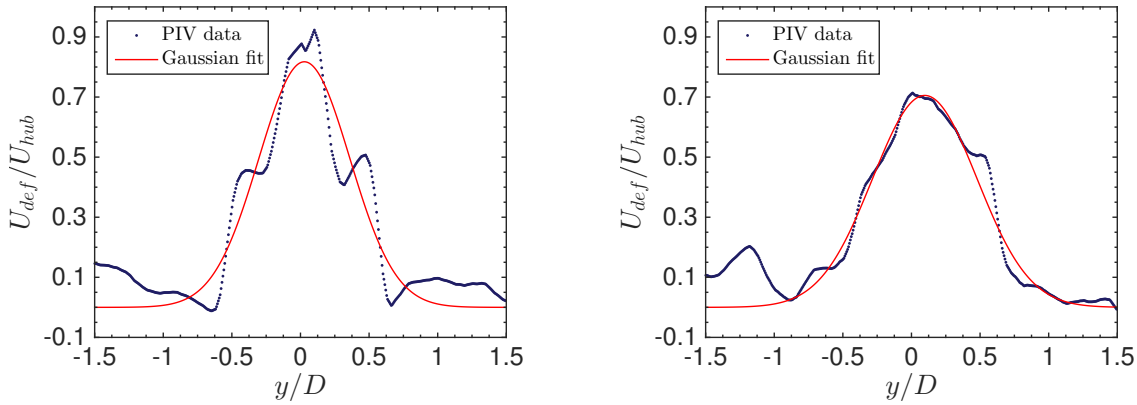

Figure 6. Gaussian fit of two normalised instantaneous wake velocity deficit profiles measured by PIV at hub height : $x = 0.5D$ (left) and $x = 3D$ (right).

4. Results and discussion

The normalised instantaneous horizontal wind speed fields obtained from PIV measurements at hub height (Fig. 7) reveal the presence of wake meandering for the three wind turbines constituting the mid row (in stream-wise direction) of the wind farm. Figure 8 presents, for each instantaneous velocity field processed, the instantaneous normalised wake-centre positions at hub height as a function of the stream-wise location. The wake-centre displacements in the y-direction appear to increase when moving downstream and reach, for some cases, the field of view limit of the CCD camera. This maximum value of $1.5D$ is not obtained because of post-processing inaccuracy but is due to "extreme deflections" of the wake (Fig. 7, bottom).

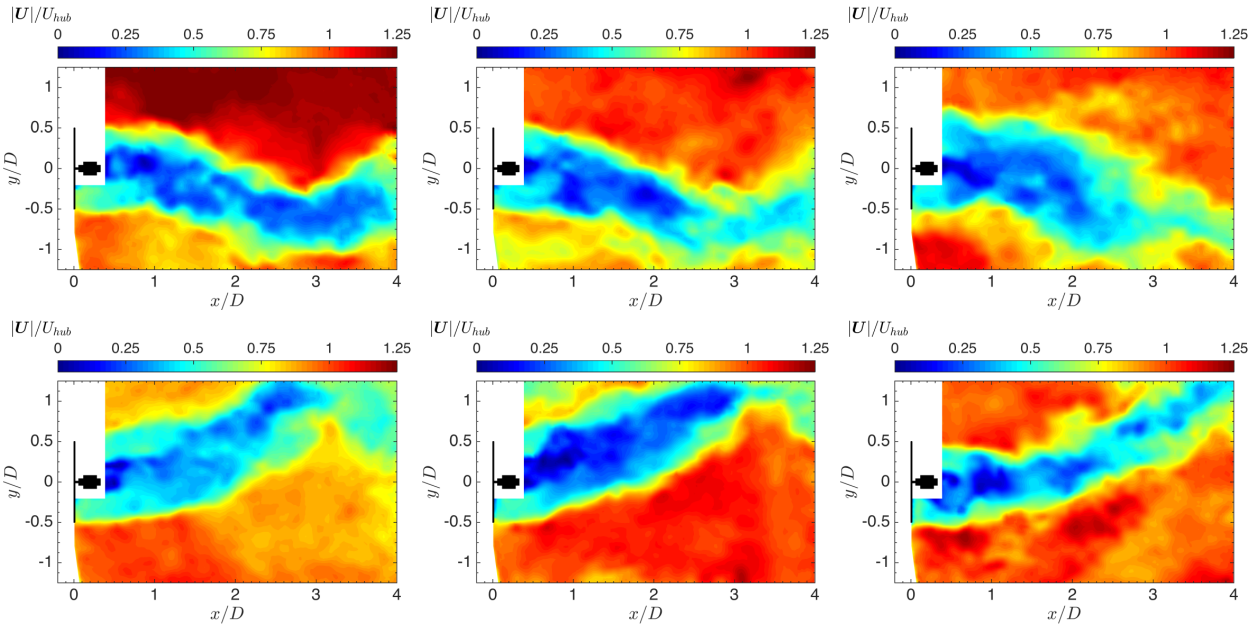

Figure 7. Normalised instantaneous horizontal wind speed ($|\boldsymbol{U}| = \sqrt{u^2 + v^2}$) fields obtained by PIV measurements at hub height at two different times revealing wake deflection : first wind turbine (left), second wind turbine (centre), and third wind turbine (right).

For each instantaneous velocity field, the wake-centreline position with reference to its time-averaged position was determined and a Fast Fourier Transform (FFT) was applied, after zero-padding, in order to obtain the characteristics of the wake-meandering phenomenon. Since the FFT was applied on a spatial signal, the resulting spectrum was obtained as a function of the

wavenumber k. The spectrum was then expressed as a function of the wavelength $\lambda = \frac{1}{k}$ and as a function of the Strouhal number by using the Taylor's frozen turbulence hypothesis

$$\left.\begin{array}{l} St = \frac{f \cdot D}{U_{hub}} \\ f = \frac{U_{hub}}{\lambda} \end{array}\right\} St = \frac{D}{\lambda}. \tag{3}$$

In order to investigate the influence of incoming wind speed on the meandering phenomenon, the same methodology was applied for measurements performed for a velocity of 4.9 m s^{-1} at hub height. The average spectra of the wake-centrelines as a function of the Strouhal number and of the frequency normalised by the wind-turbine rotational frequency f_T are showed in Fig. 9. The wake meandering characteristics, obtained from the spectra, are summarised in Table 1. Note that the meandering wavelength ($\lambda = D/St$) is of the order of $4.5D - 4.75D$, thus justifying the large field of view required for the PIV measurements.

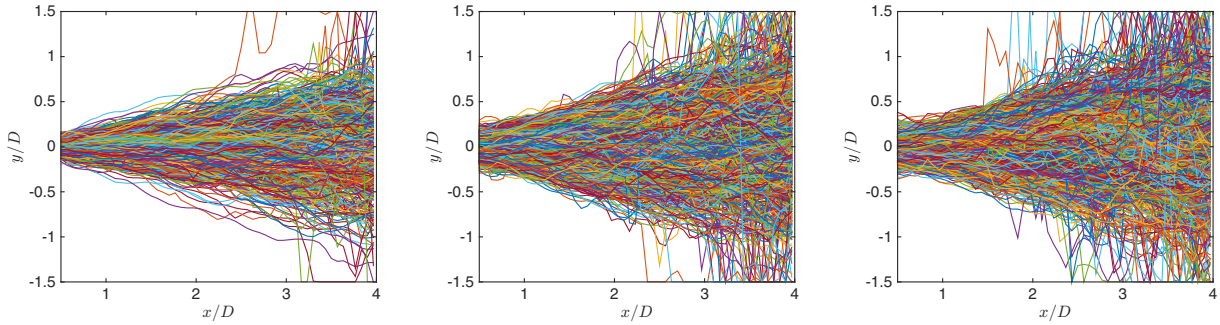

Figure 8. Normalised wake-centre positions obtained from PIV measurements at hub height as a function of the stream-wise position for each instantaneous velocity field processed : first wind turbine (left), second wind turbine (centre), and third wind turbine (right).

In order to validate the concept of the wake-centreline algorithm used in this study, the meandering characteristics obtained via PIV (spatial approach) at hub height were compared to the ones obtained from HWA (temporal approach) measurements at $x = 2D$ and at the same height (Fig.10, bottom). PIV and HWA results agree well together, particularly for the second and third turbines (Table 1). However, in the first wind-turbine wake the comparison is slightly worse because the Taylor's frozen turbulence hypothesis is probably less valid at the origin of the wake meandering. However, the excellent agreement observed between the PIV and HWA results provides an excellent proof of concept of the wake-centreline algorithm. In addition, it is interesting to note that, in contrast to what was observed by Barlas *et al.* [11, 12], the meandering phenomenon is not characterised by a well-pronounced narrow peak in the spectra but rather by a bumb spread over a larger low-frequencies range, especially at tip height (Fig.10).

		WT1		WT2		WT3	
		St	f/f_T	St	f/f_T	St	f/f_T
PIV	$U_{hub} = 4.9$ m s^{-1}	0.22	0.11	0.22	0.14	0.22	0.13
	$U_{hub} = 8.3$ m s^{-1}	0.21	0.09	0.22	0.12	0.21	0.11
HWA	$U_{hub} = 7.8$ m s^{-1}	0.14	0.06	0.22	0.11	0.20	0.10

Table 1. Meandering characteristics, Strouhal and frequency normalised by the rotor rotational frequency f_T, obtained via PIV and HWA measurements at hub height.

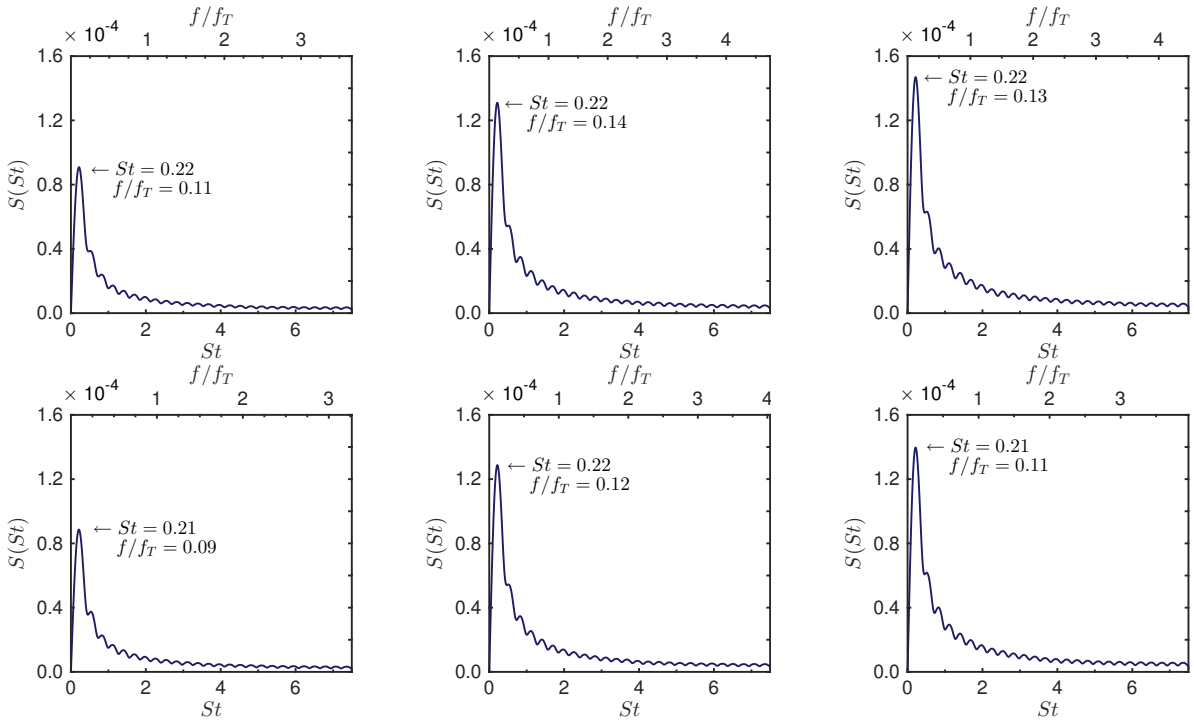

Figure 9. Average zero-padded spectra of the wake-centreline position with reference to its time-averaged position obtained from PIV measurements at hub height for $U_{hub} = 4.9$ m s^{-1} (top) and $U_{hub} = 8.3$ m s^{-1} (bottom) : first wind turbine (left), second wind turbine (centre), and third wind turbine (right). For $U_{hub} = 4.9$ m s^{-1} : $f_{T_1} = 66.7$ Hz, $f_{T_2} = 51.5$ Hz, $f_{T_3} = 54.6$ Hz and for $U_{hub} = 8.3$ m s^{-1} : $f_{T_1} = 127.2$ Hz, $f_{T_2} = 102.9$ Hz, $f_{T_3} = 105.1$ Hz.

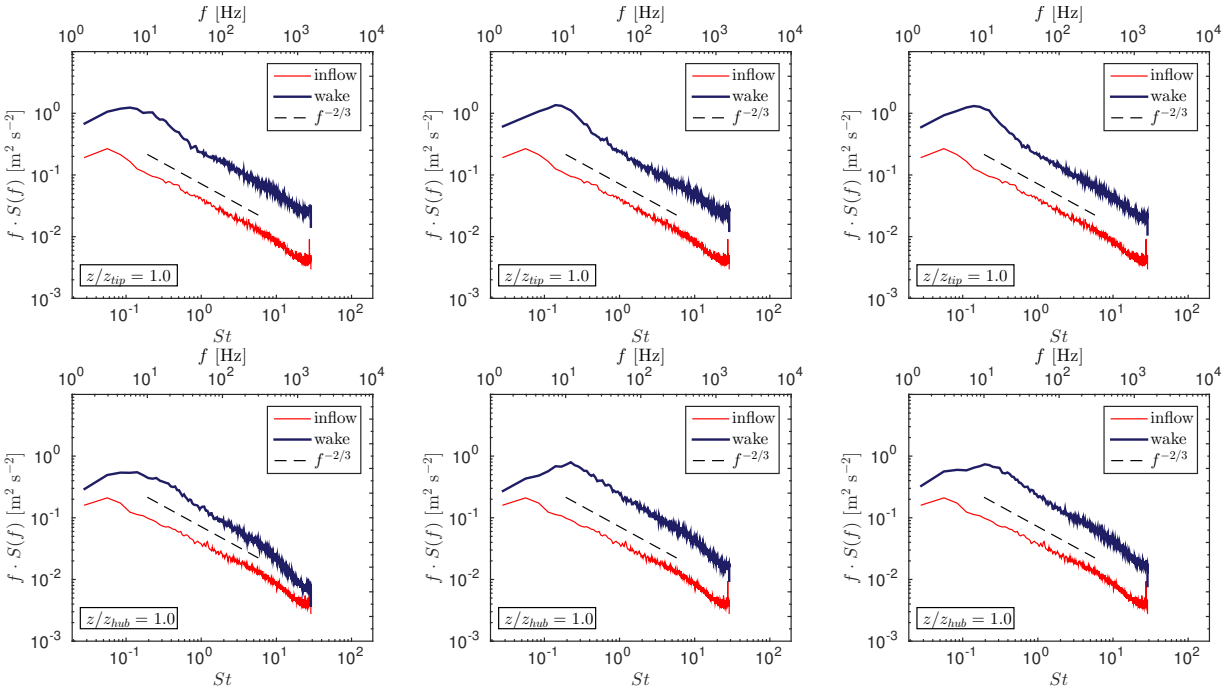

Figure 10. Comparison between the energy spectra of the inflow and at $x = 2D$ obtained from HWA measurements in the wake of the three wind turbines at $z/z_{tip} = 1.0$ (top) and $z/z_{hub} = 1.0$ (bottom) : first wind turbine (left), second wind turbine (centre), and third wind turbine (right).

5. Discussion and Conclusion

The wake-meandering phenomenon was investigated experimentally inside a 3×3 scaled wind farm placed in a neutral ABL wind tunnel inside which an ABL corresponding to a *slightly rough* terrain was modelled. PIV measurements were performed in a horizontal plane, at hub height, in the wake of the three turbines constituting the mid row (in stream-wise direction) of the scaled wind farm. Even if the PIV system employed was not able to resolve wake meandering in time, the large field of view set for the PIV camera made possible to perform a spatial analysis of the meandering structure from the velocity fields acquired. The fact that the Strouhal numbers obtained from HWA ($St = fD/U_{hub}$) and PIV ($St = D/\lambda$) are both $St \simeq 0.20 - 0.22$ proves the validity of the wake-centreline algorithm employed and the validity of the Taylor's frozen turbulence hypothesis for the wake-meandering phenomenon.

The results fall into the Strouhal numbers range $0.1 - 0.3$ obtained in various studies of wind-turbines [11–15] or hydrokinetic-turbines wakes [16]. Like in [11–14], the Strouhal number corresponding to wake meandering seems to be independent of the incoming wind speed. Furthermore, in contrast to what has been observed by Barlas *et al.* [12], the wake-meandering phenomenon persists in the wind farm and is characterised by a bumb spread over a large low-frequencies range in the HWA spectra. The differences observed are most probably due to the higher turbulence intensity of the ABL modelled in the present study : $I = 10.5\%$ vs $I = 7.5\%$ in [11, 12] at hub height. The major influence of the turbulence intensity is reinforced by the fact that, in [11, 12], no meandering was observed in the wake of a single wind turbine located in an ABL corresponding to a *rough* terrain and presenting therefore very high turbulence intensity ($I = 17.5\%$ at hub height).

Compared to literature, the wind-turbine wake meandering formation seems neither to be entirely due to intrinsic instabilities of the wake that could be associated with a periodic vortex shedding within the wake nor to be entirely due to the effects of the large scale turbulent eddies contained in the atmospheric boundary layer. The wake meandering formation seems in fact to be due to a combination of both of these propositions. Indeed, the Strouhal number obtained is in favour of the role of the intrinsic instabilities of the wake, and the fact that the phenomenon does not appear when integral length scales are smaller than the rotor diameter [6] underlines the influence of the large-scale eddies contained in the atmospheric boundary layer. The wake-meandering phenomenon seems therefore to be caused by the amplification of the intrinsic instabilities of the wake by large-scale turbulent eddies contained in the atmospheric boundary layer.

The perspectives of this work are many. The influence of the terrain roughness as well as the influence of the stability of the ABL on the wake-meandering phenomenon will be further studied. In particular, offshore and onshore ABL with various turbulence intensity levels will be modelled in the VKI Wind Engineering facility L-1B to investigate in detail the influence of the inflow on the wake-meandering phenomenon. Furthermore, the influence of the wind-turbine operating conditions on the wake meandering characteristics will be investigated.

Acknowledgments

Nicolas Coudou is funded by the *Fonds pour la Formation à la Recherche dans l'Industrie et dans l'Agriculture (FRIA)*, Belgium.

References

[1] Corbetta G, Mbistrova A, Ho A, Pineda I and Ruby K 2016 Wind in power - 2015 European statistics http://www.ewea.org/fileadmin/files/library/ publications/statistics/EWEA-Annual-Statistics-2015.pdf The European Wind Energy Association

[2] Corbetta G, Ho A, Pineda I, Ruby K and Van de Velde L 2015 Wind energy scenarios for 2030

http://www.ewea.org/fileadmin/files/library/publications/ reports/EWEA-Wind-energy-scenarios-2030.pdf The European Wind Energy Association

[3] Medici D and Alfredsson P H 2006 *Wind Energy* **9** 219–236

[4] Okulov V L and Sørensen J N 2007 *J Fluid Mech* **576** 1–25

[5] Larsen G C, Madsen H A, Thomsen K and Larsen T J 2008 *Wind Energy* **11** 377–395

[6] España G, Aubrun S, Loyer S and Devinant P 2012 *J Wind Eng Ind Aerodyn* 24–33

[7] Aubrun S, Loyer S, España G, Hayden P and Hancock P 2011 Experimental study on the wind turbine wake meandering with the help of a non-rotating simplified model and of a rotating model AIAA 2011-0460, 49th AIAA Aerospace Sciences Meeting (Orlando, FL)

[8] España G, Aubrun S, Loyer S and Devinant P 2011 *Wind Energy* **14** 923–937

[9] Muller Y A, Aubrun S and Masson C 2015 *Exp Fluids* **56** 1–11

[10] Aubrun S, Muller Y A and Masson C 2015 *Journal of Physics: Conference Series* **625**

[11] Barlas E, Buckingham S and van Beeck J 2016 *Boundary-Layer Meteorol* **158** 27–42

[12] Barlas E, Buckingham S, Glabeke G and van Beeck J 2015 Offshore and onshore wind turbine wake meandering studied in an ABL wind tunnel, International Workshop on Physical Modeling of Flow and Dispersion Phenomena (PHYSMOD) (Zürich)

[13] Medici D and Alfredsson P H 2008 *Wind Energy* **11** 211–217

[14] Okulov V, Naumov I, Mikkelsen R, Kabardin I and Sørensen J 2014 *J Fluid Mech* **747** 369–380

[15] Howard K B, Singh A, Sotiropoulos F and Guala M 2015 *Phys Fluids* **27**

[16] Chamorro L P, Hill C, Morton S, Ellis C, Arndt R E A and Sotiropoulos F 2013 *J Fluid Mech* **716** 658–670

[17] Burton T, Sharpe D, Jenkins N and Bossanyi E 2001 *Wind Energy Handbook* (John Wiley & Sons)

[18] Buckingham S 2010 Wind park siting in complex terrains assessed by wind tunnel simulations VKI PR 2010-04 von Karman Institute for Fluid Dynamics

[19] Conan B 2012 *Wind resource accessment in complex terrain by wind tunnel modelling* VKI PHDT 2013-04 Université d'Orléans - von Karman Institute for Fluid Dynamics

[20] VDI Guidelines 3783/12 2000 Physical modelling of flow and dispersion processes in the atmospheric boundary layer - Application for wind tunnels (Beuth Verlag)

[21] Eurocode 2005 EN 1991-1-4:2005 : Actions on structures - Part 1-4: General actions - Wind actions (CEN)

[22] ESDU 1985 Characteristics of atmospheric turbulence near the ground. Part II: single point data for strong winds (neutral atmosphere) Engineering Sciences Data Unit (London)

[23] Kaimal J and Finnigan J 1994 *Atmospheric Boundary Layer Flows: Their Structure and Measurement* (Oxford University Press)

[24] Scarano F 2000 *Particle Image Velocimetry - Development and Application* VKI PHDT 2000-06 von Karman Institute for Fluid Dynamics

[25] International Towing Tank Conference 2008 Recommended Procedures and Guidelines : Uncertainty Analysis - Particle Image Velocimetry 7.5-01-03-03

[26] Anthoine J, Arts T *et al* 1994 Measurements techniques in Fluid Dynamics: An Introduction Reprint of VKI LS 1994-01 Third revised edition (Von Karman Institute for Fluid Dynamics)

[27] Bingöl F, Mann J and Larsen G C 2010 *Wind Energy* **13** 51–61

[28] Trujillo J J, Bingöl F, Larsen G C, Mann J and Kühn M 2011 *Wind Energy* **14** 6175

[29] Aubrun S, Tchouaké T F, España G, Larsen G, Mann J and Bingöl F 2012 *Progress in Turbulence and Wind Energy IV: Proceedings of the iTi Conference in Turbulence 2010* (Springer Berlin Heidelberg)

[30] Vollmer L, Steinfeld G, Heinemann D and Kühn M 2016 *Wind Energy Science* **1** 129–141